



Detection of Natural Fractures from Observed Surface Seismic Data Based on a Linear-Slip Model

HUAIZHEN CHEN^{1,2}  and GUANGZHI ZHANG¹

Abstract—Natural fractures play an important role in migration of hydrocarbon fluids. Based on a rock physics effective model, the linear-slip model, which defines fracture parameters (fracture compliances) for quantitatively characterizing the effects of fractures on rock total compliance, we propose a method to detect natural fractures from observed seismic data via inversion for the fracture compliances. We first derive an approximate PP-wave reflection coefficient in terms of fracture compliances. Using the approximate reflection coefficient, we derive azimuthal elastic impedance as a function of fracture compliances. An inversion method to estimate fracture compliances from seismic data is presented based on a Bayesian framework and azimuthal elastic impedance, which is implemented in a two-step procedure: a least-squares inversion for azimuthal elastic impedance and an iterative inversion for fracture compliances. We apply the inversion method to synthetic and real data to verify its stability and reasonability. Synthetic tests confirm that the method can make a stable estimation of fracture compliances in the case of seismic data containing a moderate signal-to-noise ratio for Gaussian noise, and the test on real data reveals that reasonable fracture compliances are obtained using the proposed method.

Key words: Fracture detection, Azimuthal seismic data, Bayesian inference, Seismic inversion, Linear-slip model.

1. Introduction

Detection of natural fractures has been an important task in unconventional reservoirs (tight sand and shale reservoirs). Rock physics effective models are useful for analyzing how rock properties (porosity, minerals, saturation, etc.) affect the stiffness matrix of the rock (Mavko et al. 2009). A linear-slip model is proposed to describe the effects of

fractures on the compliance matrices of fractured rocks (Schoenberg and Douma 1988; Schoenberg and Sayers 1995). In the case of vertical or subvertical fractures embedded in a homogenous and isotropic rock, the normal and tangential fracture compliances (K_N and K_T) are defined to describe the effects of fractures on the compliance matrix. To discriminate infilling fluids in fractures, Schoenberg and Sayers (1995) suggested a fracture fluid factor, i.e., the ratio of the normal fracture compliance to the tangential fracture compliance (K_N/K_T). Bakulin et al. (2000) re-express the fracture fluid factor in terms of S-wave to P-wave velocity ratio and fracture weaknesses. Following Bakulin et al. (2000) and Chen et al. (2014) first implement seismic inversion for fracture weaknesses and then calculate the fluid factor. However, this indirect implementation accumulates errors in estimating the velocity ratio and fracture weaknesses. In the present study, we establish an efficient approach to estimate the normal and tangential fracture compliances from azimuthal seismic data.

A rock containing vertical or subvertical fractures can be considered to be a medium with horizontal transverse isotropy (HTI) (Gurevich 2003). Rüger (1997, 1998) derived a linearized PP-wave reflection coefficient for HTI media in terms of Thomsen (1986) anisotropic parameters. Using Rüger's reflection coefficient, much work has been done to predict fractures from amplitude versus offset and azimuth (AVOA) data via estimating anisotropic parameters (Chen et al. 2005; Goodway et al. 2007; Sayers 2009; Hunt et al. 2010; Far et al. 2014; Chen et al. 2014, 2017a, b). AVOA data inversion can have satisfactory results in some cases (Gray and Head 2000; Gray et al. 2003); however, if there is no better

¹ China University of Petroleum, Qingdao, Shandong, China.
E-mail: chenhz2011@gmail.com; zhanggz@upc.edu.cn

² Present Address: Department of Geoscience, University of Calgary, Calgary, AB, Canada.

constraint, it is usually unstable because AVOA data are influenced by random noise. Elastic impedance (EI), which is an extension of acoustic impedance (AI), was initially proposed by Connolly (1999). Martins (2006) derives an extended EI in terms of anisotropy parameters for weakly anisotropic media. Seismic inversion for elastic properties (P- and S-wave impedances, velocities, density, etc.) has been divided into two procedures: EI inversion from seismic data stacked over incidence angles, and estimation of elastic properties from the inversion results of EI. Seismic inversion based on EI has the advantage of both improving the signal-to-noise ratio (SNR) owing to the stack processing (Liu et al. 2009) and making the estimation of elastic properties more stable, because the input inversion results of EI contain no effects of wavelets (Chen et al. 2014). In this paper, we derive azimuthal EI in terms of fracture compliances and implement seismic inversion for fracture compliances based on the derived azimuthal EI.

Shaw and Sen (2004, 2006) present a method to derive linearized reflection coefficients for weakly anisotropic media using a scattering function and perturbation in stiffness matrix. Following Shaw and Sen (2004, 2006), we first express perturbations in stiffness parameters in terms of fracture compliances for the case of an interface separating two media that contain vertical or subvertical fractures. Using the scattering function and the perturbations, we derive a linearized PP-wave reflection coefficient and azimuthal EI in terms of fracture compliances. Using the derived azimuthal EI, we establish a two-step inversion method to estimate fracture compliances, which involves a model-constrained and damped least-squares inversion for EI at different azimuths and an iterative inversion for fracture compliances based on a Bayesian framework. We apply the established method to synthetic and real data sets to validate their stability and reasonability.

2. Theory and Method

2.1. Perturbations in Stiffness Parameters

Schoenberg and Douma (1988) present the linear-slip model to express the compliance matrix **S** of a fractured rock:

$$\mathbf{S} = \mathbf{S}_{\text{iso}} + \mathbf{S}_f, \tag{1}$$

where \mathbf{S}_{iso} is the compliance matrix of the isotropic background, and \mathbf{S}_f is fracture excess compliance.

For the case of a rock containing rotationally invariant vertical fractures (Shaw and Sen 2004, 2006), \mathbf{S}_f is given by Schoenberg and Sayers (1995) and Gurevich (2003) as:

$$\mathbf{S}_f = \begin{bmatrix} Z_N & 0 & 0 & 0 & 0 & 0 \\ 0 & 0 & 0 & 0 & 0 & 0 \\ 0 & 0 & 0 & 0 & 0 & 0 \\ 0 & 0 & 0 & 0 & 0 & 0 \\ 0 & 0 & 0 & 0 & Z_T & 0 \\ 0 & 0 & 0 & 0 & 0 & Z_T \end{bmatrix}, \tag{2}$$

where Z_N and Z_T are the normal and tangential fracture compliances.

Inverting the compliance matrix **S** yields stiffness matrix **C** in terms of fracture compliances:

$$\mathbf{C} = \mathbf{S}^{-1} = \begin{bmatrix} \lambda + 2\mu & \lambda & \lambda & 0 & 0 & 0 \\ \lambda & \lambda + 2\mu & \lambda & 0 & 0 & 0 \\ \lambda & \lambda & \lambda + 2\mu & 0 & 0 & 0 \\ 0 & 0 & 0 & \mu & 0 & 0 \\ 0 & 0 & 0 & 0 & \mu & 0 \\ 0 & 0 & 0 & 0 & 0 & \mu \end{bmatrix} - \begin{bmatrix} \frac{(\lambda+2\mu)^2 Z_N}{1+(\lambda+2\mu)Z_N} & \frac{\lambda(\lambda+2\mu)Z_N}{1+(\lambda+2\mu)Z_N} & \frac{\lambda(\lambda+2\mu)Z_N}{1+(\lambda+2\mu)Z_N} & 0 & 0 & 0 \\ \frac{\lambda(\lambda+2\mu)Z_N}{1+(\lambda+2\mu)Z_N} & \frac{\lambda^2 Z_N}{1+(\lambda+2\mu)Z_N} & \frac{\lambda^2 Z_N}{1+(\lambda+2\mu)Z_N} & 0 & 0 & 0 \\ \frac{\lambda(\lambda+2\mu)Z_N}{1+(\lambda+2\mu)Z_N} & \frac{\lambda^2 Z_N}{1+(\lambda+2\mu)Z_N} & \frac{\lambda^2 Z_N}{1+(\lambda+2\mu)Z_N} & 0 & 0 & 0 \\ 0 & 0 & 0 & 0 & 0 & 0 \\ 0 & 0 & 0 & 0 & \frac{\mu^2 Z_T}{1+\mu Z_T} & 0 \\ 0 & 0 & 0 & 0 & 0 & \frac{\mu^2 Z_T}{1+\mu Z_T} \end{bmatrix}, \tag{3}$$

where λ and μ are Lamé constants of the isotropic background.

Schoenberg and Douma (1988) demonstrate two approximations, $\frac{(\lambda+2\mu)Z_N}{1+(\lambda+2\mu)Z_N} \approx (\lambda + 2\mu)Z_N$ and $\frac{\mu Z_T}{1+\mu Z_T} \approx \mu Z_T$, under assumptions of $(\lambda +$

$2\mu)Z_N \ll 1$ and $\mu Z_T \ll 1$; hence, Eq. (3) is approximately written as:

$$\mathbf{C} \approx \begin{bmatrix} \lambda + 2\mu & \lambda & \lambda & 0 & 0 & 0 \\ \lambda & \lambda + 2\mu & \lambda & 0 & 0 & 0 \\ \lambda & \lambda & \lambda + 2\mu & 0 & 0 & 0 \\ 0 & 0 & 0 & \mu & 0 & 0 \\ 0 & 0 & 0 & 0 & \mu & 0 \\ 0 & 0 & 0 & 0 & 0 & \mu \end{bmatrix} - \begin{bmatrix} (\lambda + 2\mu)^2 Z_N & \lambda(\lambda + 2\mu)Z_N & \lambda(\lambda + 2\mu)Z_N & 0 & 0 & 0 \\ \lambda(\lambda + 2\mu)Z_N & \lambda^2 Z_N & \lambda^2 Z_N & 0 & 0 & 0 \\ \lambda(\lambda + 2\mu)Z_N & \lambda^2 Z_N & \lambda^2 Z_N & 0 & 0 & 0 \\ 0 & 0 & 0 & 0 & 0 & 0 \\ 0 & 0 & 0 & 0 & \mu^2 Z_T & 0 \\ 0 & 0 & 0 & 0 & 0 & \mu^2 Z_T \end{bmatrix}. \tag{4}$$

Using the approximate expression for the stiffness matrix in Eq. (4), we present the perturbation in the stiffness matrix: where $\Delta\lambda$, $\Delta\mu$, ΔZ_N , and ΔZ_T are changes in Lamé constants and fracture compliances across the interface. Under assumptions of small changes in Lamé constants and fracture compliances

$$\Delta\mathbf{C} = \begin{bmatrix} \Delta\lambda + 2\Delta\mu & \Delta\lambda & \Delta\lambda & 0 & 0 & 0 \\ \Delta\lambda & \Delta\lambda + 2\Delta\mu & \Delta\lambda & 0 & 0 & 0 \\ \Delta\lambda & \Delta\lambda & \Delta\lambda + 2\Delta\mu & 0 & 0 & 0 \\ 0 & 0 & 0 & \Delta\mu & 0 & 0 \\ 0 & 0 & 0 & 0 & \mu & 0 \\ 0 & 0 & 0 & 0 & 0 & \mu \end{bmatrix} - \begin{bmatrix} (\lambda + 2\mu)^2 \Delta Z_N & \lambda(\lambda + 2\mu)\Delta Z_N & \lambda(\lambda + 2\mu)\Delta Z_N & 0 & 0 & 0 \\ \lambda(\lambda + 2\mu)\Delta Z_N & \lambda^2 \Delta Z_N & \lambda^2 \Delta Z_N & 0 & 0 & 0 \\ \lambda(\lambda + 2\mu)\Delta Z_N & \lambda^2 \Delta Z_N & \lambda^2 \Delta Z_N & 0 & 0 & 0 \\ 0 & 0 & 0 & 0 & 0 & 0 \\ 0 & 0 & 0 & 0 & \mu^2 \Delta Z_T & 0 \\ 0 & 0 & 0 & 0 & 0 & \mu^2 \Delta Z_T \end{bmatrix}, \tag{5}$$

and weak fracture compliances, we ignore the items proportional to $\Delta\lambda(Z_N + \Delta Z_N)$, $\Delta\mu(Z_N + \Delta Z_N)$, $\Delta\mu(Z_T + \Delta Z_T)$, $(\Delta\lambda)^2$ and $(\Delta\mu)^2$ in the derivation of the perturbation in the stiffness matrix. It is important to stress that we assume the rock contains a

set of vertical fractures and the vertical fractures have only one dominant azimuth.

2.2. Linearized PP-Wave Reflection Coefficient and Azimuthal Elastic Impedance

Shaw and Sen (2004, 2006) present an approach to use scattering function and perturbations in stiffness parameters to derive linearized reflection coefficients for weakly anisotropic media. The PP-wave reflection coefficient is given by:

$$R_{PP} = \frac{1}{4\rho \cos^2 \theta} \begin{pmatrix} \Delta\rho\xi + \Delta C_{11}\Gamma_{11} + \Delta C_{12}\Gamma_{12} + \Delta C_{13}\Gamma_{13} \\ + \Delta C_{21}\Gamma_{12} + \Delta C_{22}\Gamma_{22} + \Delta C_{23}\Gamma_{23} \\ + \Delta C_{31}\Gamma_{13} + \Delta C_{32}\Gamma_{23} + \Delta C_{33}\Gamma_{33} \\ + \Delta C_{44}\Gamma_{44} + \Delta C_{55}\Gamma_{55} + \Delta C_{66}\Gamma_{66} \end{pmatrix}, \tag{6}$$

where ρ is density, $\Delta\rho$ is its perturbation, and θ is the angle of incidence, and where $\xi = \cos 2\theta/V_P^2$, $\Gamma_{11} = \sin^4 \theta \cos^4 \phi/V_P^2$, $\Gamma_{12} = \sin^4 \theta \sin^2 \phi \cos^2 \phi/V_P^2$, $\Gamma_{13} = \sin^2 \theta \cos^2 \theta \cos^2 \phi/V_P^2$, $\Gamma_{22} = \sin^4 \theta \sin^4 \phi/V_P^2$, $\Gamma_{23} = \sin^2 \theta \cos^2 \theta \sin^2 \phi/V_P^2$, $\Gamma_{33} = \cos^4 \theta/V_P^2$, $\Gamma_{44} = -4 \sin^2 \theta \cos^2 \theta \sin^2 \phi/V_P^2$, $\Gamma_{55} = -4 \sin^2 \theta$

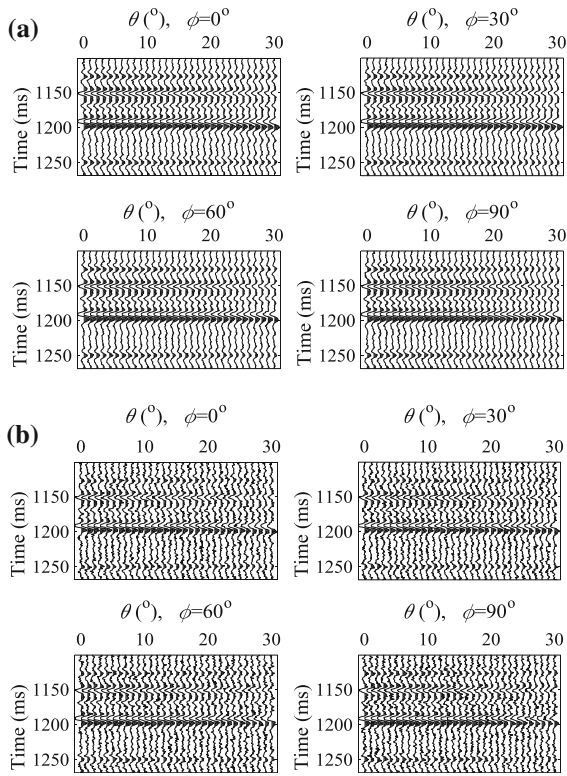


Figure 1

Noisy seismic angle gathers. **a** SNR = 5, and **b** SNR = 2

$\cos^2 \theta \cos^2 \phi / V_P^2$, $\Gamma_{66} = 4 \sin^4 \theta \sin^2 \phi \cos^2 \phi / V_P^2$, in which ϕ is the azimuth, and V_P is the P-wave velocity of the isotropic background.

Incorporating Eqs. (5)–(6), we derive the expression of PP-wave reflection coefficient:

$$R_{PP}(\theta, \phi) = a_P(\theta)R_P + a_S(\theta)R_S + a_D(\theta)R_D + a_{Z_N}(\theta, \phi)\Delta Z_N + a_{Z_T}(\theta, \phi)\Delta Z_T, \quad (7)$$

where $a_P(\theta) = \sec^2 \theta$, $a_S(\theta) = -8g \sin^2 \theta$, $a_D(\theta) = 4g \sin^2 \theta - \tan^2 \theta$, $a_{Z_N}(\theta, \phi) = -\frac{\mu g}{4 \cos^2 \theta} \left[\frac{1}{g} - 2(\sin^2 \theta \sin^2 \phi + \cos^2 \theta) \right]^2$, and $a_{Z_T}(\theta, \phi) = \mu g \sin^2 \theta \cos^2 \phi (1 - \tan^2 \theta \sin^2 \phi)$, and where $R_P = \frac{\Delta I_P}{2I_P}$, $R_S = \frac{\Delta I_S}{2I_S}$ and $R_D = \frac{\Delta \rho}{2\rho}$ are P-wave impedance (I_P), S-wave impedance (I_S), and density (ρ) reflectivities, and ΔI_P and ΔI_S are changes in P- and S-wave impedances across the interface. In practice, the quantities μ and g are provided by well-logging data. Following Buland and Omre (2003), we extend the derived PP-wave reflection coefficient as a time-continuous function:

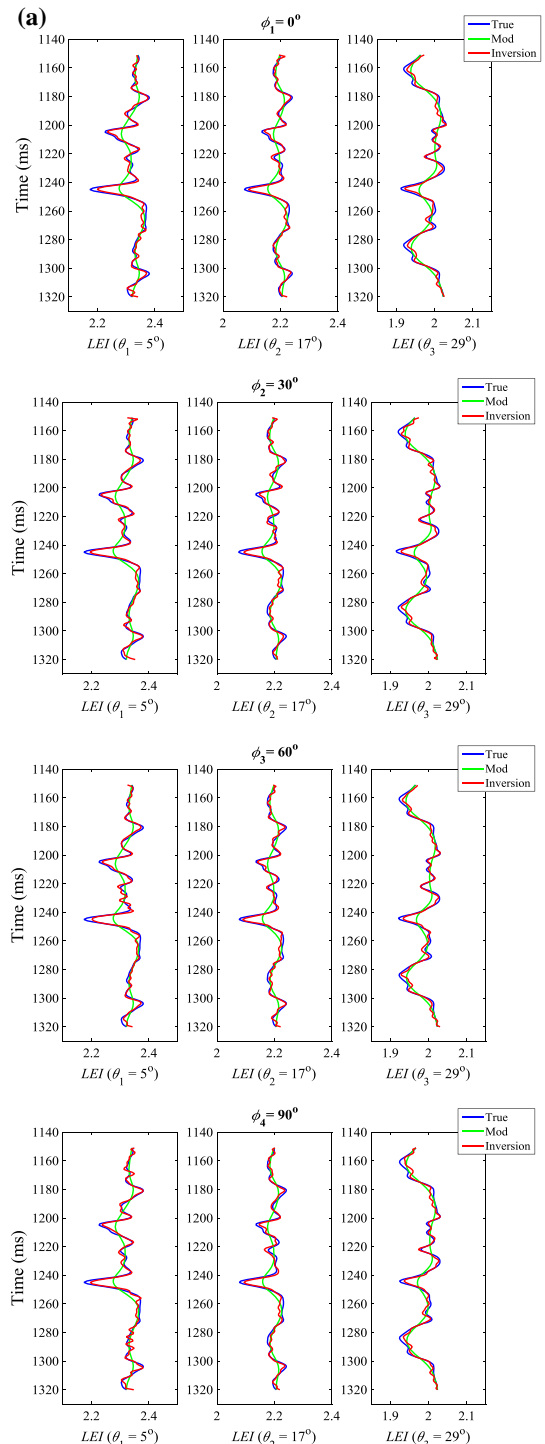


Figure 2

Comparisons between true values (blue) and inversion results (red) of logarithmic EI. **a** SNR = 5, and **b** SNR = 2. The green curve represents the initial model of logarithmic EI which is the smoothed version of the true value

$$\begin{aligned}
 R_{PP}(t, \theta, \phi) = & \frac{1}{2} a_P(t, \theta) \frac{\partial}{\partial t} \ln I_P(t) + \frac{1}{2} a_S(t, \theta) \frac{\partial}{\partial t} \ln I_S(t) \\
 & + \frac{1}{2} a_D(t, \theta) \frac{\partial}{\partial t} \ln \rho(t) \\
 & + \frac{1}{2} a_{Z_N}(t, \theta, \phi) \frac{\partial}{\partial t} Z_N(t) + \frac{1}{2} a_{Z_T} \\
 & (t, \theta, \phi) \frac{\partial}{\partial t} Z_T(t),
 \end{aligned} \tag{8}$$

where $I_P(t)$, $I_S(t)$, $\rho(t)$, $Z_N(t)$, and $Z_T(t)$ are time samples of P-wave impedance, S-wave impedance, density, and the normal and tangential fracture compliances.

Combining the relationship between reflection coefficient and EI ($R_{PP} \approx \frac{1}{2} \frac{\Delta EI}{EI} \approx \frac{1}{2} \frac{\partial}{\partial t} \text{LEI}$) and taking a time integral operation for Eq. (8), we express the logarithmic EI (LEI) as:

$$\begin{aligned}
 \text{LEI}(t, \theta, \phi) = & a_P(t, \theta) \ln I_P(t) + a_S(t, \theta) \ln I_S(t) \\
 & + a_D(t, \theta) \ln \rho(t)
 \end{aligned} \tag{9}$$

The expression of azimuthal EI is given by:

$$\begin{aligned}
 \text{EI}(t, \theta, \phi) = & I_P(t)^{a_P(t, \theta)} I_S(t)^{a_S(t, \theta)} \rho(t)^{a_D(t, \theta)} \exp[a_{Z_N}(t, \theta, \phi) Z_N(t) \\
 & + a_{Z_T}(t, \theta, \phi) Z_T(t)],
 \end{aligned} \tag{10}$$

where $\exp[\]$ denotes the exponential function.

2.3. Azimuthal Elastic Impedance Inversion and Fracture Compliance Estimation

Implementation of seismic inversion for fracture compliances involves azimuthal EI inversion from seismic data stacked over the incidence angle and estimation of fracture compliances from the inversion results of azimuthal EI. The convolution model can be used to generate seismic data vector \mathbf{B} using a wavelet vector \mathbf{W} and logarithmic EI vector \mathbf{X} :

$$\mathbf{B} = \mathbf{C}\mathbf{X}, \tag{11}$$

where

$$\mathbf{B} = \begin{bmatrix} B(t_1, \theta, \phi) \\ B(t_2, \theta, \phi) \\ \vdots \\ B(t_{NN}, \theta, \phi) \end{bmatrix}, \mathbf{C} = \frac{1}{2} \mathbf{W}\mathbf{D},$$

$$\mathbf{X} = \begin{bmatrix} \text{LEI}(t_1, \theta, \phi) \\ \text{LEI}(t_2, \theta, \phi) \\ \vdots \\ \text{LEI}(t_{NN}, \theta, \phi) \end{bmatrix}, \mathbf{D} \text{ is a difference operation}$$

matrix given by

$$\mathbf{D} = \begin{bmatrix} -1 & 1 & 0 & \dots \\ 0 & -1 & 1 & 0 \\ 0 & 0 & -1 & 1 \\ 0 & 0 & 0 & \dots \end{bmatrix}, \text{ and } NN \text{ is the number}$$

of time samples.

A model-based and damped least-squares inversion algorithm is employed to solve Eq. (11) to obtain the logarithmic EI:

$$\mathbf{X} = \mathbf{X}_{\text{mod}} + (\mathbf{C}^T \mathbf{C} + \tau \mathbf{I})^{-1} \mathbf{C}^T (\mathbf{B} - \mathbf{C}\mathbf{X}_{\text{mod}}), \tag{12}$$

where \mathbf{X}_{mod} is a given smooth initial model, \mathbf{I} is a unit matrix, τ is a damping factor, and T is transpose of a matrix.

After obtaining the logarithmic EI, we proceed to the estimation of fracture compliances using an iterative inversion method based on the Bayesian framework. Using Eq. (9), the relation between the logarithmic EI and unknown parameters (P- and S-wave impedances, density, and fracture compliances) is succinctly expressed as:

$$\mathbf{d} = \mathbf{G}\mathbf{m}, \tag{13}$$

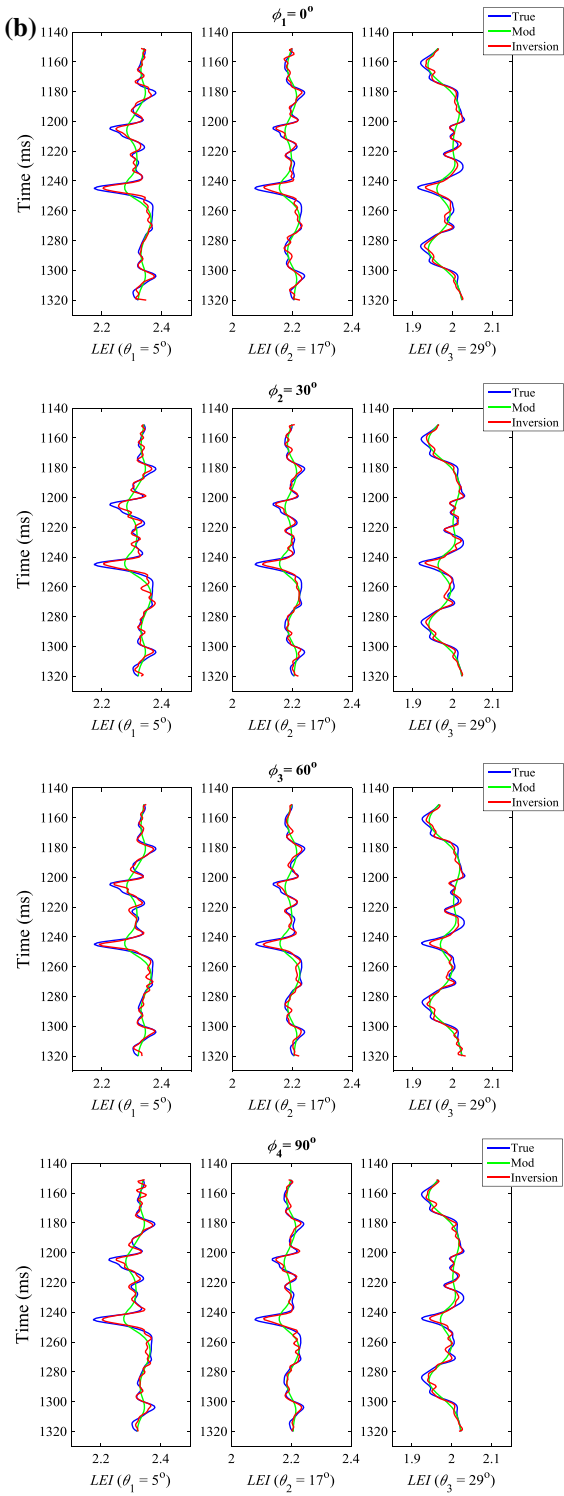
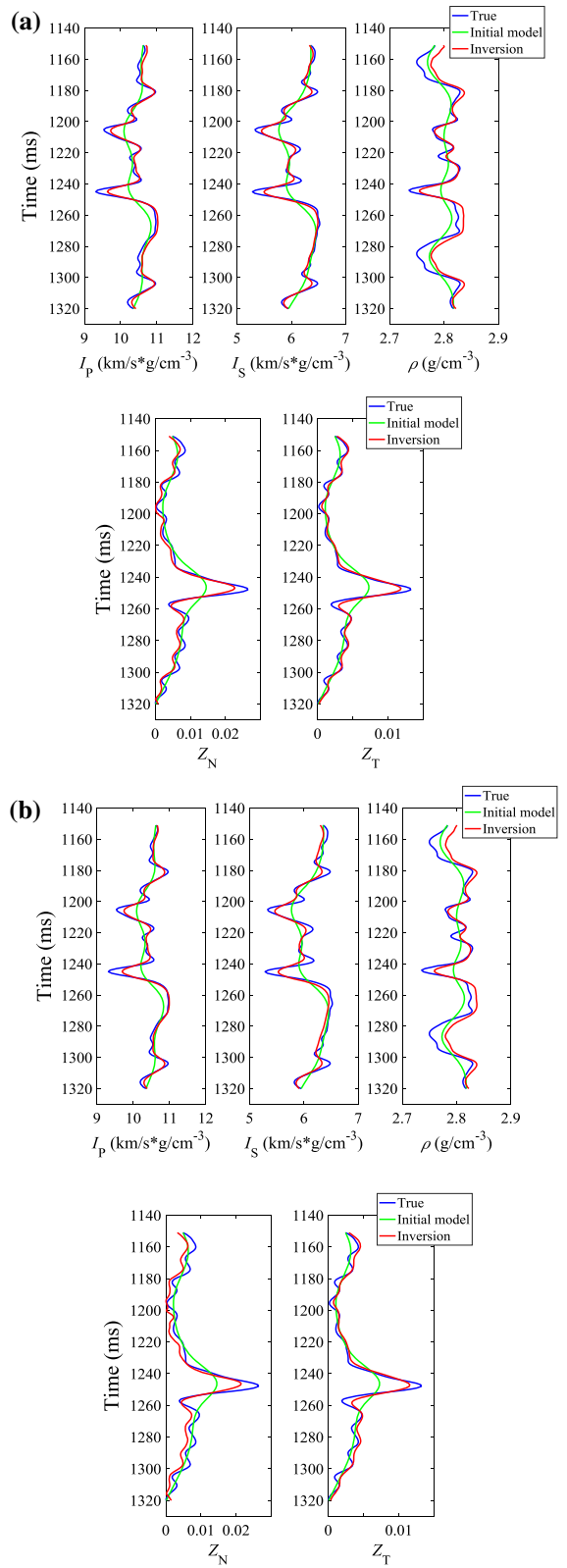


Figure 2 continued



◀Figure 3

Comparisons between true values (blue) and inversion results (red) of P- and S-wave impedances, density, and fracture compliances. **a** SNR = 5, and **b** SNR = 2. The green curve represents the initial model, which is the smoothed version of the true value

where

$$\mathbf{d} = \begin{bmatrix} \mathbf{LEI}(\theta_1, \phi_1) & \mathbf{LEI}(\theta_2, \phi_1) & \mathbf{LEI}(\theta_3, \phi_1) \\ \cdots & \mathbf{LEI}(\theta_1, \phi_M) & \mathbf{LEI}(\theta_2, \phi_M) \\ & & \mathbf{LEI}(\theta_3, \phi_M) \end{bmatrix}^T$$

$$\mathbf{m} = [\mathbf{L}_P \quad \mathbf{L}_S \quad \mathbf{L}_D \quad \mathbf{Z}_N \quad \mathbf{Z}_T]^T, \text{ and}$$

$$\mathbf{G} = \begin{bmatrix} \mathbf{A}_P(\theta_1) & \mathbf{A}_S(\theta_1) & \mathbf{A}_D(\theta_1) & \mathbf{A}_{Z_N}(\theta_1, \phi_1) & \mathbf{A}_{Z_T}(\theta_1, \phi_1) \\ \mathbf{A}_P(\theta_2) & \mathbf{A}_S(\theta_2) & \mathbf{A}_D(\theta_2) & \mathbf{A}_{Z_N}(\theta_2, \phi_1) & \mathbf{A}_{Z_T}(\theta_2, \phi_1) \\ \mathbf{A}_P(\theta_3) & \mathbf{A}_S(\theta_3) & \mathbf{A}_D(\theta_3) & \mathbf{A}_{Z_N}(\theta_3, \phi_1) & \mathbf{A}_{Z_T}(\theta_3, \phi_1) \\ \vdots & \vdots & \vdots & \vdots & \vdots \\ \mathbf{A}_P(\theta_1) & \mathbf{A}_S(\theta_1) & \mathbf{A}_D(\theta_1) & \mathbf{A}_{Z_N}(\theta_1, \phi_M) & \mathbf{A}_{Z_T}(\theta_1, \phi_M) \\ \mathbf{A}_P(\theta_2) & \mathbf{A}_S(\theta_2) & \mathbf{A}_D(\theta_2) & \mathbf{A}_{Z_N}(\theta_2, \phi_M) & \mathbf{A}_{Z_T}(\theta_2, \phi_M) \\ \mathbf{A}_P(\theta_3) & \mathbf{A}_S(\theta_3) & \mathbf{A}_D(\theta_3) & \mathbf{A}_{Z_N}(\theta_3, \phi_M) & \mathbf{A}_{Z_T}(\theta_3, \phi_M) \end{bmatrix}$$

and where, $\mathbf{LEI} = [\mathbf{LEI}(t_1) \quad \cdots \quad \mathbf{LEI}(t_{NN})]^T$,
 $\mathbf{L}_P = [\ln I_P(t_1) \quad \cdots \quad \ln I_P(t_{NN})]^T$, $\mathbf{L}_S = [\ln I_S(t_1) \quad \cdots \quad \ln I_S(t_{NN})]^T$, $\mathbf{L}_D = [\ln \rho(t_1) \quad \cdots \quad \ln \rho(t_{NN})]^T$,
 $\mathbf{Z}_N = [\mathbf{Z}_N(t_1) \quad \cdots \quad \mathbf{Z}_N(t_{NN})]^T$, $\mathbf{Z}_T = [\mathbf{Z}_T(t_1) \quad \cdots \quad \mathbf{Z}_T(t_{NN})]^T$, $\mathbf{A}_P = \text{diag}[a_P(t_1)$

$\cdots a_P(t_{NN})]$, $\mathbf{A}_S = \text{diag}[a_S(t_1) \cdots a_S(t_{NN})]$, $\mathbf{A}_D = \text{diag}[a_D(t_1) \cdots a_D(t_{NN})]$, $\mathbf{A}_{Z_N} = \text{diag}[a_{Z_N}(t_1) \cdots a_{Z_N}(t_{NN})]$, and $\mathbf{A}_{Z_T} = \text{diag}[a_{Z_T}(t_1) \cdots a_{Z_T}(t_{NN})]$. The incidence angles, θ_1 , θ_2 and θ_3 , represent near, middle and far incident angles.

Bayesian theory is used to construct the objective function for estimating the unknown parameter vector \mathbf{m} from the input data (i.e., the inversion results of logarithmic EI at different azimuthal angles). The posterior probability distribution function (PDF), $P(\mathbf{m}|\mathbf{d})$, of the unknown parameter vector is given by:

$$P(\mathbf{m}|\mathbf{d}) \propto P(\mathbf{d}|\mathbf{m})P(\mathbf{m}), \quad (14)$$

where $P(\mathbf{d}|\mathbf{m})$ and $P(\mathbf{m})$ are the likelihood function

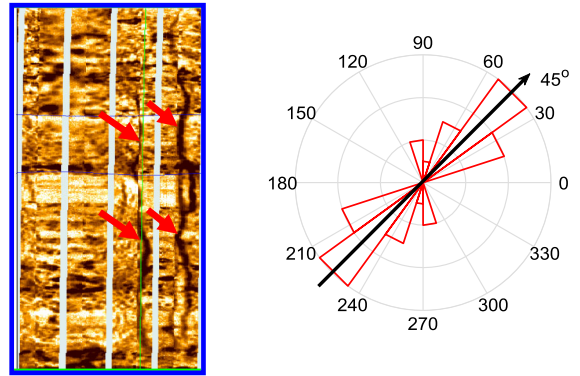


Figure 5

Formation MicroImager (FMI) log picture and fracture azimuth rose diagram. Fractures are marked by red arrows in the FMI log picture

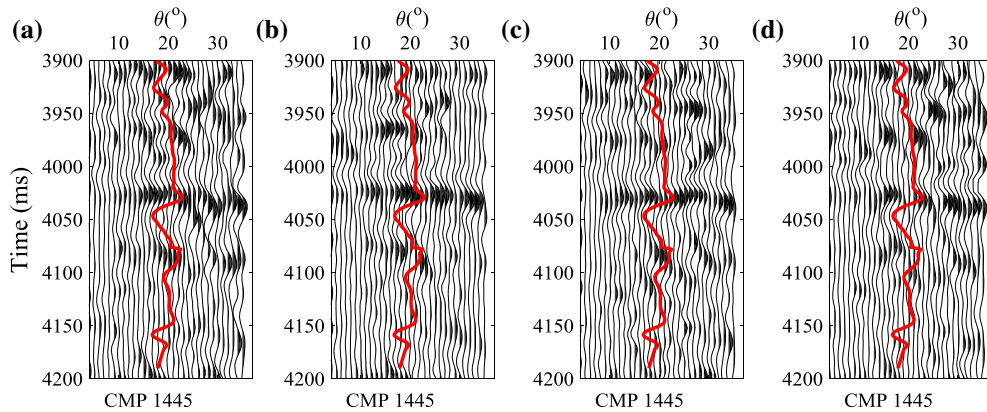


Figure 4

Seismic angle gathers at different azimuths. **a** $\phi_1 = 10^\circ$, **b** $\phi_1 = 30^\circ$, **c** $\phi_1 = 150^\circ$, and **d** $\phi_1 = 170^\circ$

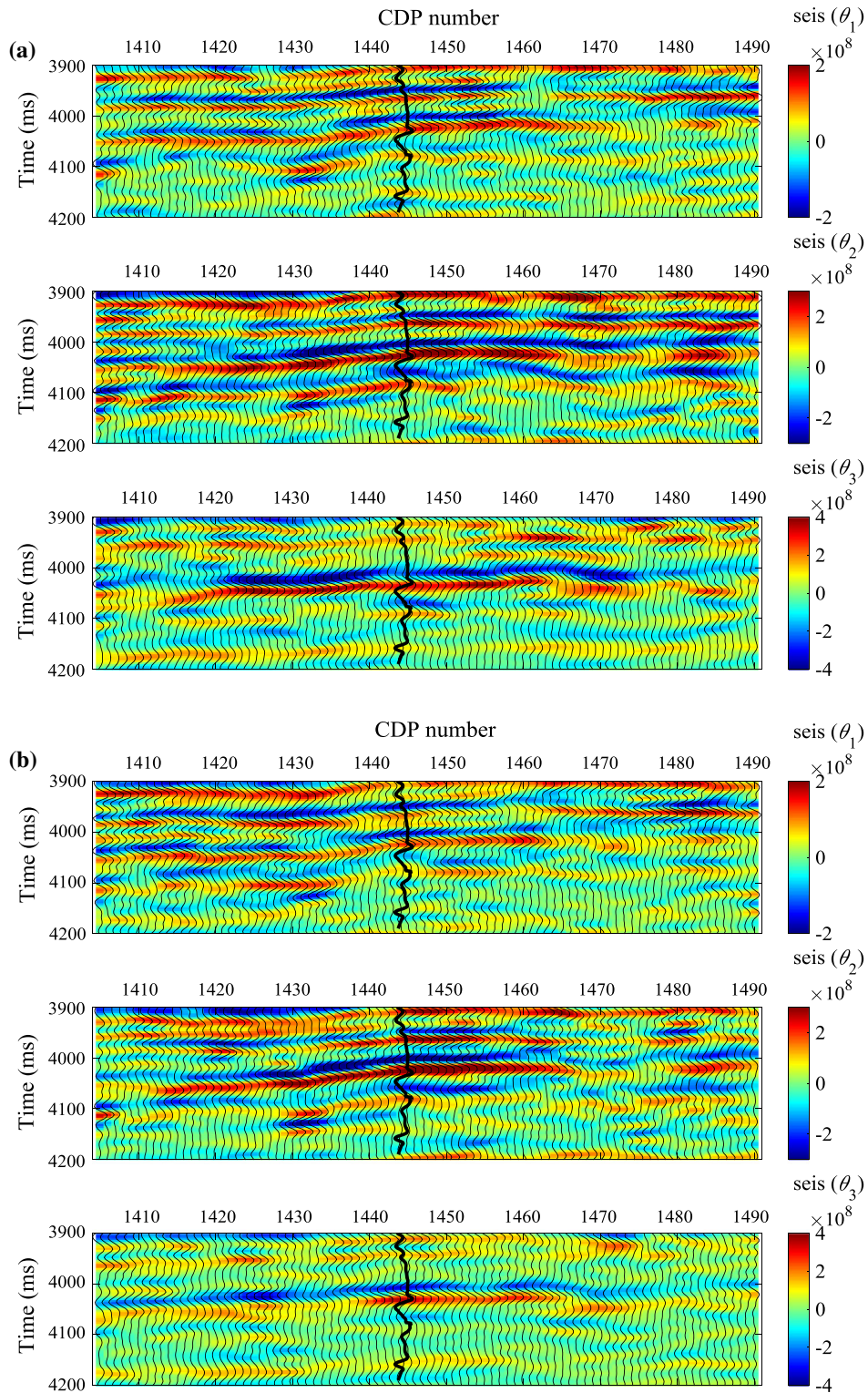


Figure 6

Stacked seismic profiles at different azimuths. **a** $\phi_1 = 10^\circ$, **b** $\phi_1 = 30^\circ$, **c** $\phi_1 = 150^\circ$, and **d** $\phi_1 = 170^\circ$. The curves represent P-wave velocity

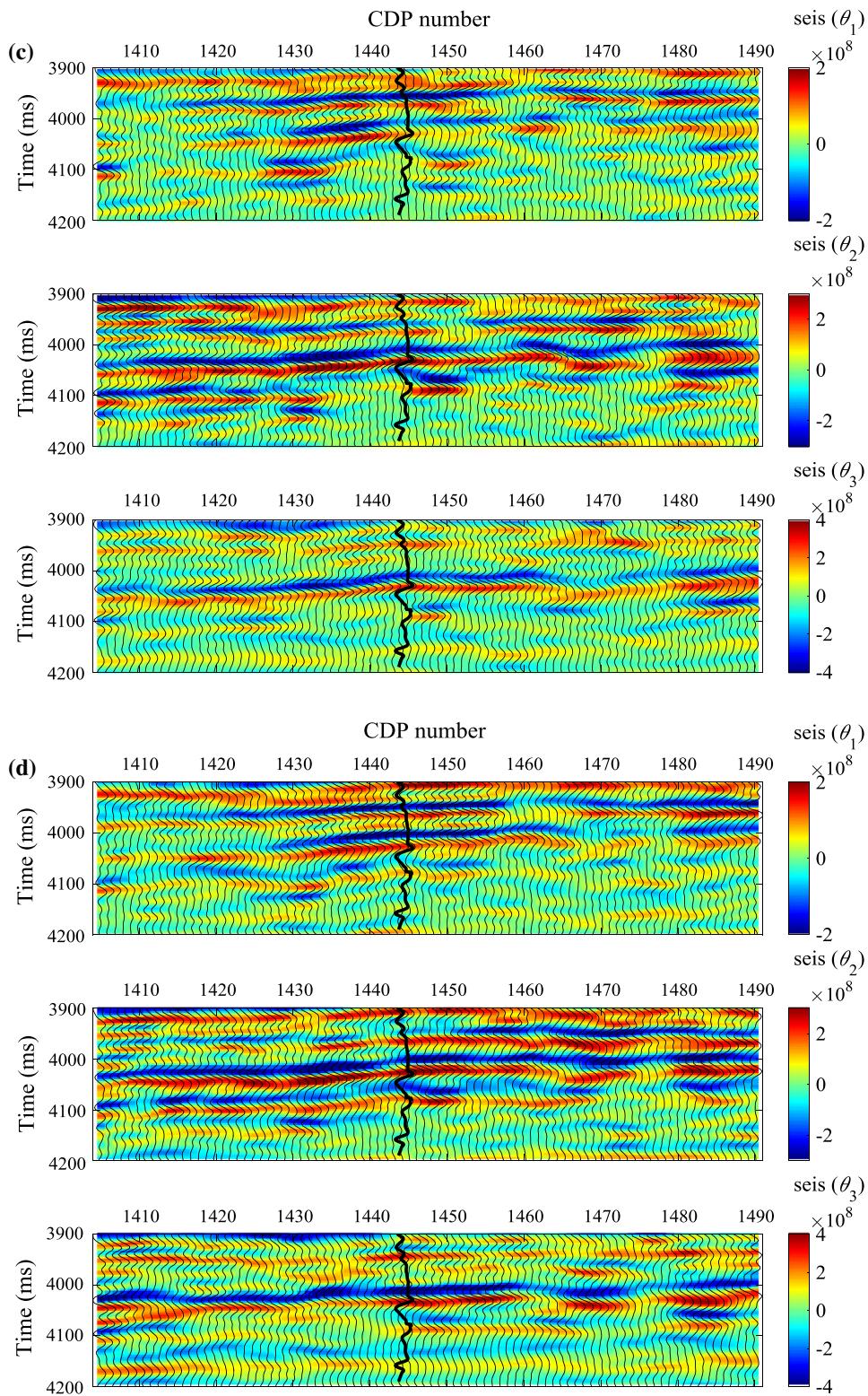


Figure 6 continued

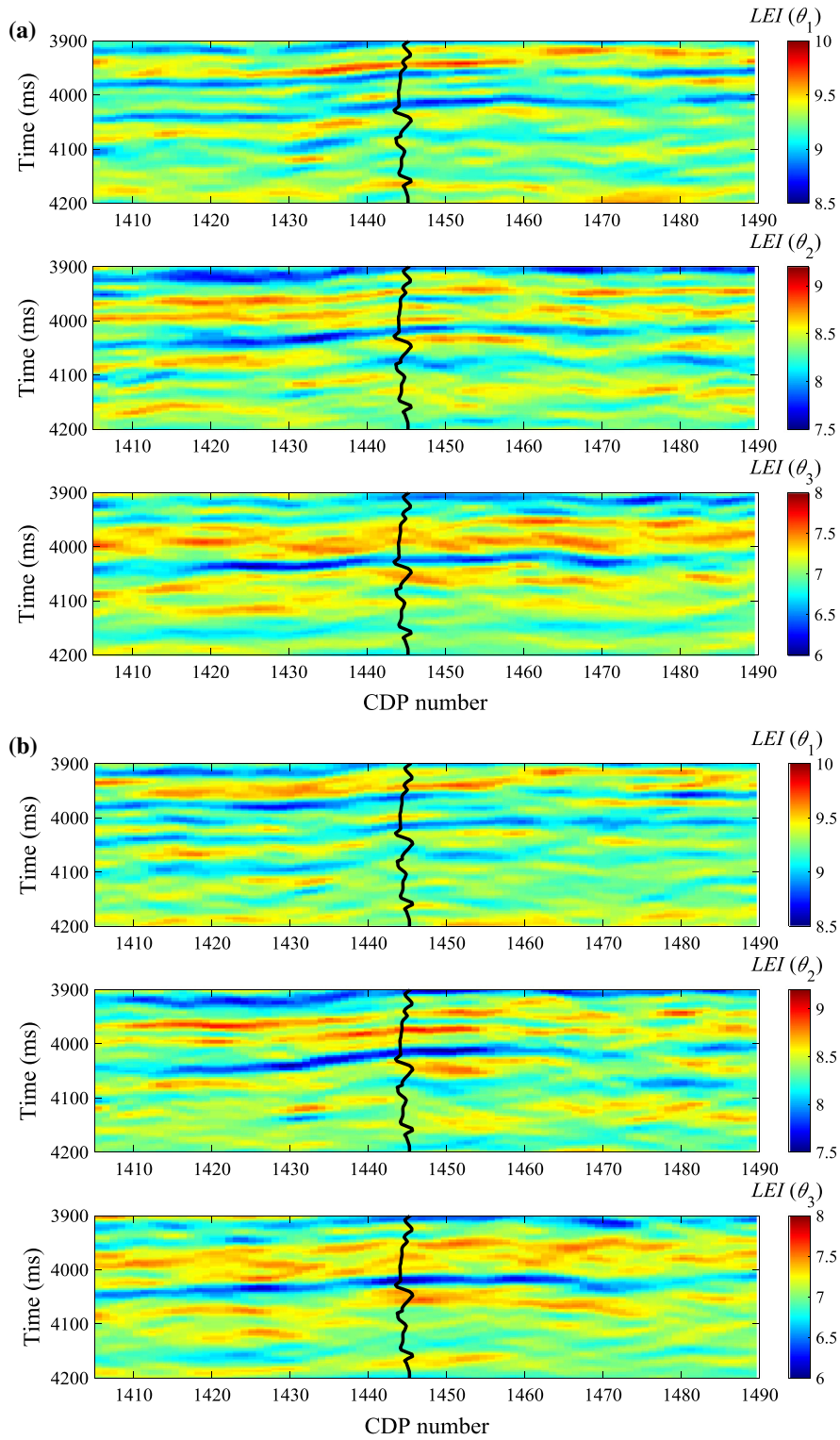


Figure 7

Inversion results of logarithmic EI at different azimuths. **a** $\phi_1 = 10^\circ$, **b** $\phi_1 = 30^\circ$, **c** $\phi_1 = 150^\circ$, and **d** $\phi_1 = 170^\circ$. The curve plotted in each figure is P-wave velocity from well log data

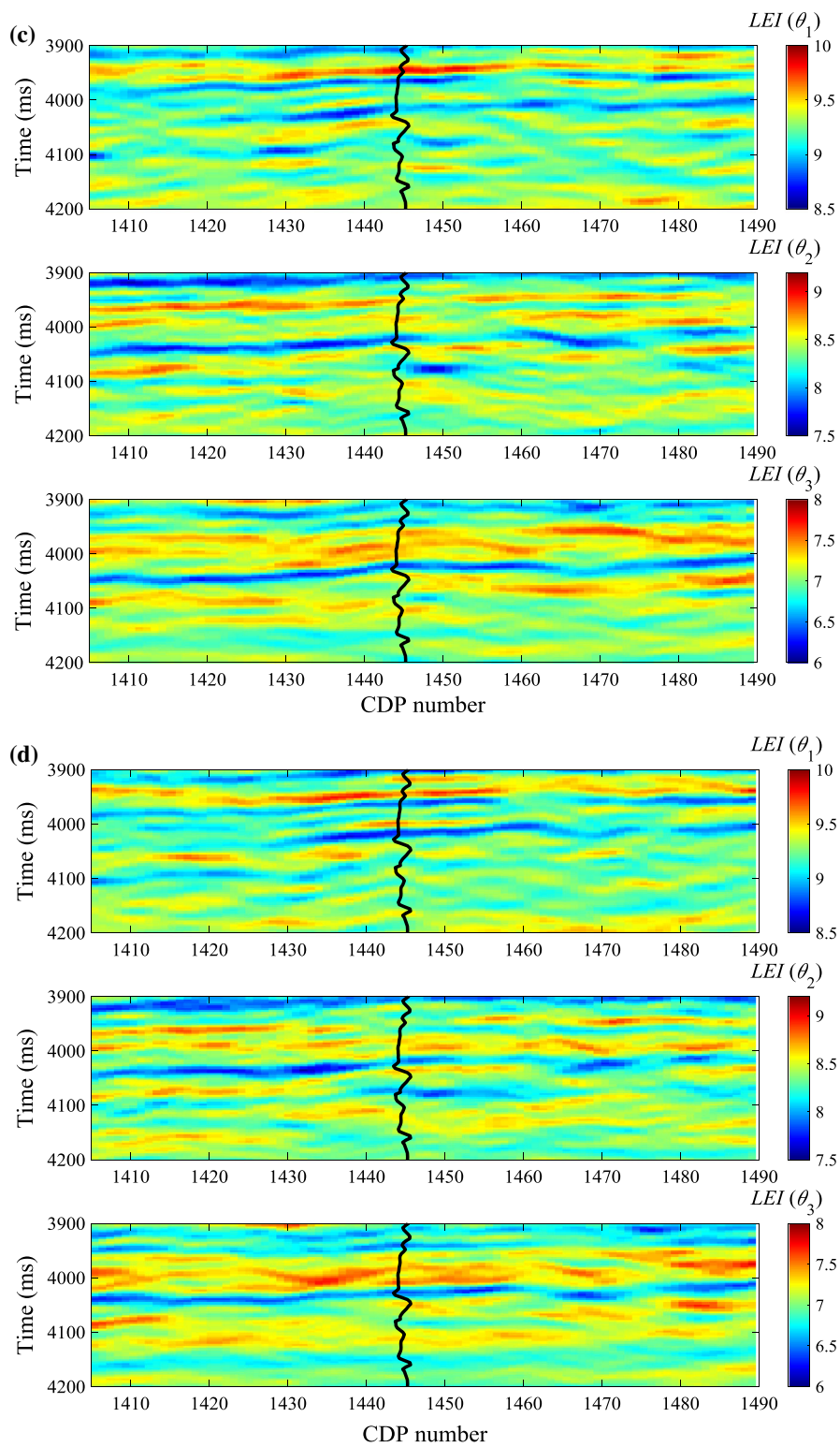


Figure 7 continued

and the prior information PDF, respectively. The likelihood function depends on differences between the input data and the synthetic data predicted for a given unknown parameter vector. Assuming the probability distribution of the difference to be Gaussian, we express the likelihood function as:

$$P(\mathbf{d}|\mathbf{m}) = \frac{1}{\sqrt{(2\pi)^{NN}(\sigma_{\text{error}}^2)^{NN}}} \exp\left[\sum \frac{-(\mathbf{d} - \mathbf{Gm})^T(\mathbf{d} - \mathbf{Gm})}{2\sigma_{\text{error}}^2}\right], \quad (15)$$

where σ_{error}^2 is the variance of the difference.

We employ Cauchy distribution prior information, which can produce sparse results that have a high-resolution (Downton 2005; Alemie and Sacchi 2011):

$$P(\mathbf{m}) = \frac{1}{(\pi^2\sigma_{\mathbf{m}})^{NN}} \exp\left[-2 \sum \ln\left(1 + \frac{\mathbf{m}^2}{\sigma_{\mathbf{m}}^2}\right)\right], \quad (16)$$

where $\sigma_{\mathbf{m}}^2$ is the covariance of the unknown parameter vector.

Combining Eqs. (15) and (16), we obtain the expression of the posterior PDF. Maximizing the posterior PDF can produce the solution of the inversion problem (Alemie and Sacchi 2011), which means minimizing the function $J(\mathbf{m})$ involved in the posterior PDF. The expression for $J(\mathbf{m})$ is given by:

$$J(\mathbf{m}) = \sum \frac{(\mathbf{d} - \mathbf{Gm})^T(\mathbf{d} - \mathbf{Gm})}{2\sigma_{\text{error}}^2} + 2 \sum \ln\left(1 + \frac{\mathbf{m}^2}{\sigma_{\mathbf{m}}^2}\right). \quad (17)$$

To obtain the unknown parameter vector \mathbf{m} that minimizes the function $J(\mathbf{m})$, we need to solve the following equation

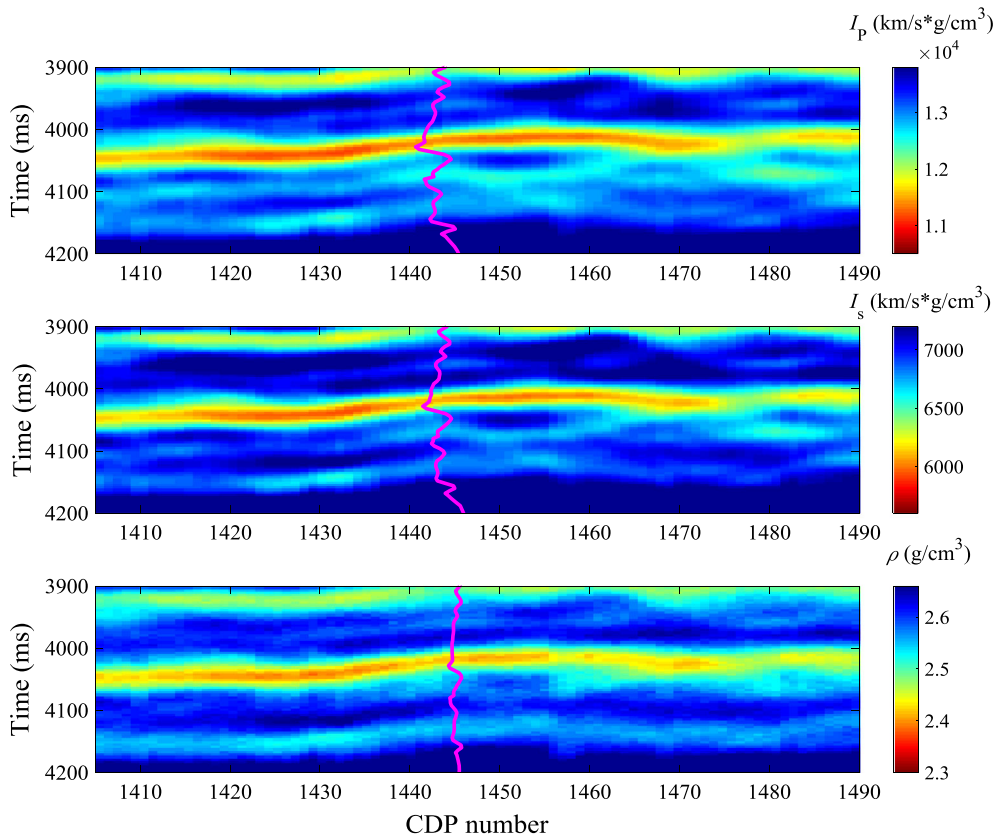


Figure 8

Inversion results of P- and S-wave impedances and density. The corresponding curve from well log data is plotted in the profile of inversion result

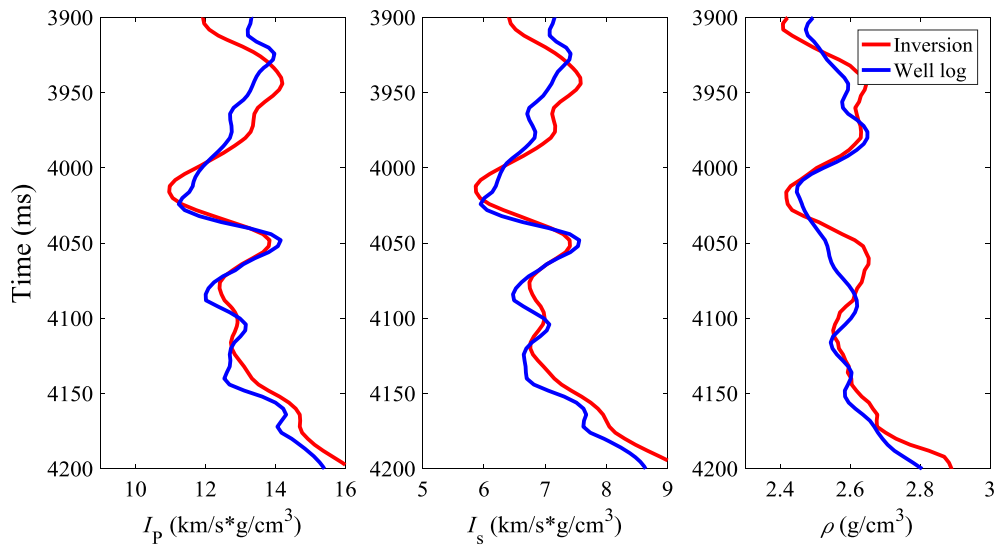


Figure 9

Comparisons between inversion results (red) and well log curves (blue) of P- and S-wave impedances and density

$$\frac{\partial[J(\mathbf{m})]}{\partial \mathbf{m}} = 0. \quad (18)$$

$$\left(\mathbf{G}^T \mathbf{G} + \frac{4\sigma_{\text{error}}^2}{\sigma_{\mathbf{m}}^2 + \mathbf{m}^2} \right) \mathbf{m} = \mathbf{G}^T \mathbf{d}. \quad (19)$$

After applying some algebraic operations, Eq. (18) can be further expressed as:

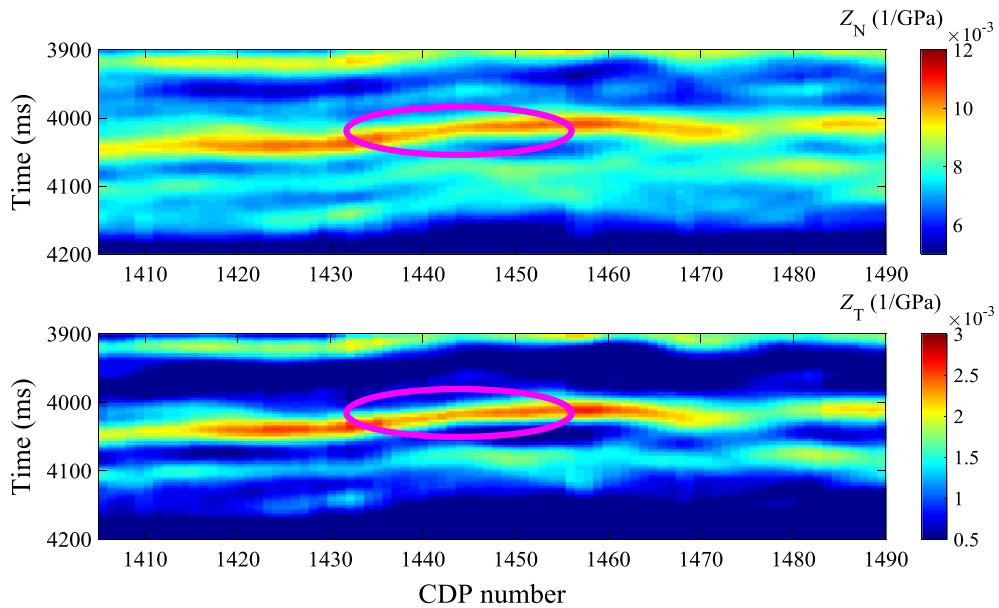


Figure 10

Inversion results of the normal and tangential fracture compliances. The ellipse represents the location of the fractured reservoir

Because Eq. (19) is nonlinear, we employ an iterative approach to obtain the solution of the unknown parameter vector:

$$\mathbf{m}_{i+1} = \left(\mathbf{G}^T \mathbf{G} + \frac{4\sigma_{\text{error}}^2}{\sigma_{\mathbf{m}}^2 + \mathbf{m}_i^2} \right)^{-1} \mathbf{G}^T \mathbf{d}, \quad (20)$$

where \mathbf{m}_{i+1} is the calculated result based on the i th solution \mathbf{m}_i . P- and S-wave impedances and density in the initial solution \mathbf{m}_1 are constructed using well log data, and for real data inversion, the normal and tangential fracture compliances in the initial solution \mathbf{m}_1 are assumed to be zero.

3. Results

3.1. Synthetic Test

Using the convolution model based on Eqs. (9) and (11) and a 40 Hz Ricker wavelet, we first use a well log model to generate synthetic seismic gathers at different incidence angles and azimuths. Given a constant fracture density, we construct fracture compliances of the well log model using elastic parameters (P- and S-wave impedances and density) and expressions of dry fracture compliances (Appendix). Using an incidence angle range of 0° – 30° , and four azimuths $\phi_1 = 0^\circ$, $\phi_2 = 30^\circ$, $\phi_3 = 60^\circ$, and $\phi_4 = 90^\circ$, we first generate seismic angle gathers, and then we stack the seismic gathers over different incidence angle ranges to obtain small ($\theta_1 = 5^\circ$ stacked over the range 0° – 10°), middle ($\theta_2 = 15^\circ$ stacked over the range 10° – 20°), and large ($\theta_3 = 25^\circ$ stacked over the range 20° – 30°) incidence angle seismic data. To verify the robustness of the proposed approach, we add Gaussian random noise with different SNRs (SRNs are 5 and 2, respectively) into synthetic seismic gathers. Figure 1 shows noisy synthetic seismic angle gathers.

Using the small, middle and large angle stacked seismic data at different azimuths; we implement the inversion for azimuthal logarithmic EI. Comparisons between true values of logarithmic EI calculated using Eq. (9) and inversion results obtained by the model-based and damped least-squares inversion algorithm as discussed in the previous section are shown in Fig. 2.

From Fig. 2, we observe that the logarithmic EI can be estimated stably even in the case of the SNR being 2. With the estimated logarithmic EI in hand, we proceed to the inversion for P- and S-wave impedances, density, and fracture compliances, and we show comparisons between true values and inversion results in Fig. 3. We use the smoothed version of the unknown parameter (i.e., P- and S-wave impedances, density and fracture compliances) as the initial model (green curves) in the inversion.

From Fig. 3, we see that P- and S-wave impedances and fracture compliances can be estimated reasonably. However, the accuracy of density inversion should be improved by involving more large-offset data.

3.2. Real Data

Real data acquired in Northwest China are employed to implement azimuthal EI inversion and fracture compliances extraction to further verify the proposed approach. For the data, the incidence angle range for each common-midpoint-profile (CMP) gather is 4° – 37° . In Fig. 4, we plot angle gathers at CMP 1445, in which a P-wave velocity curve (red) is added. We find there is an anomalous amplitude (around 4020 ms) which has been proved to be a fractured and gas-bearing reservoir by a Formation MicroImager (FMI) log as shown in Fig. 5. We also show fracture azimuth estimated using a method of amplitude versus offset and azimuth (AVOA) analysis presented by Chen et al. (2017a, b).

From Fig. 5, we observe that there are some vertical or subvertical fractures in this reservoir, which confirms the assumption of HTI media. We stack seismic angle gathers over different angle ranges to obtain small ($\theta_1 = 9^\circ$ stacked over the range 4° – 14°), middle ($\theta_1 = 20^\circ$ stacked over the range 15° – 25°) and large ($\theta_1 = 31^\circ$ stacked over the range 26° – 37°) angle seismic profiles, as shown in Fig. 6.

From Fig. 6, we observe a “bright-spot” anomaly and structural high around 4020 ms in the vicinity of the drilled well. Using the model-based and damped least-squares inversion algorithm discussed in the previous section, we invert the stacked seismic

profiles at different azimuths for the logarithmic EI. It is important to stress that, assuming fracture compliances are zero, we use the P- and S-wave impedances and density of the well-logging data to calculate the logarithmic EI, and the smoothed result of the calculated logarithmic EI is used as the initial model in the logarithmic EI inversion for all azimuths. For the case of complicated subsurface structure, Chen et al. (2017a, b) presented the approach of constructing initial models using a commercial software package. The inversion results of logarithmic EI are displayed in Fig. 7.

From Fig. 7, we see that the inversion result of logarithmic EI show a low value in the location of the reservoir (around 4020 ms, CDP 1445). After obtaining the results of logarithmic EI, we proceed to the iterative inversion for fracture compliances. To implement the inversion, we use the smoothed version of well log data as initial models for P- and S-wave impedances and density, and we let initial models of fracture compliances be zero. Inversion results of P- and S-wave impedances and density are shown in Fig. 8. We observe that the inversion results of P- and S-wave impedances and density show relatively low values in the location of fractured reservoirs, and there is a reasonable match between the inversion result and the well log curve, as shown in Fig. 9.

We next plot inversion results of the normal and tangential fracture compliances in Fig. 10. From these inversion results, we observe that both the normal and tangential fracture compliances show high values in the vicinity of the fractured reservoir. These inversion results can be used to detect fracture distribution and calculate the fracture fluid factor.

4. Conclusions

Motivated by the fracture fluid factor defined in terms of fracture compliances, we have established an efficient approach to estimate fracture compliances from observed seismic data based on azimuthal EI. The assumptions under which we implemented this research are that the rock contains a set of vertical fractures and the vertical fractures have only one dominant azimuth. Based on the linear-slip model,

we first express perturbations in stiffness parameters in terms of fracture compliances. Combining these perturbations and the scattering function, we derive a linearized PP-wave reflection coefficient and azimuthal EI as a function of fracture compliances. The inversion for fracture compliances is implemented in a two-step approach, which involves a model-based and damped least-squares inversion for azimuthal EI from seismic data stacked over different incidence angle ranges at different azimuths, and an iterative inversion for P- and S-wave impedances, density, and fracture compliances from the estimated results of azimuthal EI. Applying the approach to noisy synthetic seismic data confirms that the inversion for P- and S-wave impedances and fracture compliances is stable in the case of seismic data containing a moderate SNR noise. A test on real data shows that reasonable results of P- and S-wave impedances and fracture compliances can be obtained and P- and S-wave impedances show relatively low values and fracture compliances show relatively high values in the location of fractured reservoirs.

Acknowledgements

We would like to acknowledge the support from SINOPEC Key Lab of Multi-Component Seismic Technology. We want to thank David Henley who is working in CREWES Project, University of Calgary, for helping us to improve the editing and writing. We also thank the reviewers for their valuable and constructive suggestions and the editor Dr. Andrew Gorman for handling this paper.

Appendix: Expressions of Dry Fracture Compliances

Using relationships between fracture compliances and fracture weaknesses (Bakulin et al. 2000), we derive expressions of dry fracture compliances in terms of Lamé constants and fracture density:

$$\begin{aligned} Z_N &= \frac{4e}{3\mu(\lambda + \mu) - 4e(\lambda + 2\mu)}, \\ Z_T &= \frac{16e}{3\mu(3\lambda + 4\mu) - 16e\mu}, \end{aligned} \quad (21)$$

where e is fracture density.

Lamé constants are expressed as:

$$\begin{aligned}\mu &= (I_S)^2 / \rho \\ \lambda &= (I_P)^2 / \rho - 2(I_S)^2 / \rho\end{aligned}\quad (22)$$

REFERENCES

- Alemie, W., & Sacchi, M. D. (2011). High-resolution three-term AVO inversion by means of a Trivariate Cauchy probability distribution. *Geophysics*, *76*, R43–R55.
- Bakulin, A., Grechka, V., & Tsvankin, I. (2000). Estimation of fracture parameters from reflection seismic data—part I: HTI model due to a single fracture set. *Geophysics*, *65*, 1788–1802.
- Buland, A., & Omre, H. (2003). Bayesian linearized AVO inversion. *Geophysics*, *68*, 185–198.
- Chen, H., Brown, R. L., & Castagna, J. P. (2005). AVO for one- and two fracture set models. *Geophysics*, *70*, C1–C5.
- Chen, H., Ji, Y., & Innanen, K. (2017a). Estimation of modified fluid factor and dry fracture weaknesses using azimuthal elastic impedance. *Geophysics*, *83*(1), WA73–WA88.
- Chen, H., Zhang, G., Chen, J., & Yin, X. (2014). Fracture filling fluids identification using azimuthally elastic impedance based on rock physics. *Journal of Applied Geophysics*, *110*, 98–105.
- Chen, H., Zhang, G., Ji, Y., & Yin, X. (2017b). Azimuthal seismic amplitude difference inversion for fracture weakness. *Pure and Applied Geophysics*, *174*, 279–291.
- Connolly, P. (1999). Elastic impedance. *The Leading Edge*, *18*, 438–452.
- Downton, J. (2005). Seismic parameter estimation from AVO inversion. Ph.D. Thesis, University of Calgary.
- Far, M. E., Hardage, B., & Wagner, D. (2014). Fracture parameter inversion for Marcellus Shale. *Geophysics*, *79*, C55–C63.
- Goodway, B., Varsek, J., Abaco, C. (2007). Anisotropic 3D Amplitude variation with azimuth (AVAZ) methods to detect fracture prone zones in tight gas resource plays. *CSPG/CSEG Convention*, 590–596.
- Gray, D., Boerner, S., & Marinic, D. T. (2003). Fractured reservoir characterization using AVAZ on the Pinedale anticline, Wyoming. *CSEG Recorder*, *33*, 41–46.
- Gray, D., & Head, K. (2000). Fracture detection in Manderson field: a 3-D AVAZ case history. *The Leading Edge*, *11*, 1214–1221.
- Gurevich, B. (2003). Elastic properties of saturated porous rocks with aligned fractures. *Journal of Applied Geophysics*, *54*, 203–218.
- Hunt, L., Reynolds, S., & Brown, T. (2010). Quantitative estimate of fracture density variations in the Nordegg with azimuthal AVO and curvature: a case study. *The Leading Edge*, *29*, 1122–1137.
- Liu, G., Fomel, S., Jin, L., & Chen, X. (2009). Stacking seismic data using local correlation. *Geophysics*, *74*, V43–V48.
- Martins, J. L. (2006). Elastic impedance in weakly anisotropic media. *Geophysics*, *71*, D73–D83.
- Mavko, G., Mukerji, T., & Dvorkin, J. (2009). *The rock physics hand book-second edition*. UK: Cambridge University Press.
- Rüger, A. (1997). P-wave reflection coefficients for transversely isotropic models with vertical and horizontal axis of symmetry. *Geophysics*, *62*, 713–722.
- Rüger, A. (1998). Variation of P-wave reflectivity with offset and azimuth in anisotropic media. *Geophysics*, *63*, 935–947.
- Sayers, C. M. (2009). Seismic characterization of reservoirs containing multiple fracture sets. *Geophysical Prospecting*, *57*, 187–192.
- Schoenberg, M., & Douma, J. (1988). Elastic wave propagation in media with parallel vertical fractures and aligned cracks. *Geophysical Prospecting*, *36*, 571–590.
- Schoenberg, M., & Sayers, C. M. (1995). Seismic anisotropy of fractured rock. *Geophysics*, *60*, 204–211.
- Shaw, R. K., & Sen, M. K. (2004). Born integral, stationary phase and linearized reflection coefficients in weak anisotropic media. *Geophysical Journal International*, *158*, 225–238.
- Shaw, R. K., & Sen, M. K. (2006). Use of AVOA data to estimate fluid indicator in a vertically fractured medium. *Geophysics*, *71*, C15–C24.
- Thomsen, L. (1986). Weak elastic anisotropy. *Geophysics*, *51*, 1954–1966.

(Received July 12, 2017, revised March 19, 2018, accepted March 20, 2018, Published online March 30, 2018)